ELSEVIER

Materials Science and Engineering A319–321 (2001) 854–861

MATERIALS SCIENCE & ENGINEERING A

www.elsevier.com/locate/msea

On the effect of grain size on yield stress: extension into nanocrystalline domain

David J. Benson, Hsueh-Hung Fu, Marc André Meyers *

Department of Mechanical and Aerospace Engineering, University of California San Diego, La Jolla, CA 92093, USA

Abstract

Four principal factors contribute to grain-boundary strengthening: (a) the grain boundaries act as barriers to plastic flow; (b) the grain boundaries act as dislocation sources; (c) elastic anisotropy causes additional stresses in grain-boundary surroundings; (d) multislip is activated in the grain-boundary regions, whereas grain interiors are initially dominated by single slip, if properly oriented. As a result, the regions adjoining grain boundaries harden at a rate much higher than grain interiors. A phenomenological constitutive equation predicting the effect of grain size on the yield stress of metals is discussed and extended to the nanocrystalline regime. At large grain sizes, it has the Hall–Petch form, and in the nanocrystalline domain the slope gradually decreases until it asymptotically approaches the flow stress of the grain boundaries. The material is envisaged as a composite, comprised of the grain interior, with flow stress σ_{fB} and grain boundary work-hardened layer, with flow stress σ_{fGB}. The predictions of this model are compared with experimental measurements over the mono, micro, and nanocrystalline domains. Computational predictions are made of plastic flow as a function of grain size incorporating differences of dislocation accumulation rate in grain-boundary regions and grain interiors. The material is modeled as a monocrystalline core surrounded by a mantle (grain-boundary region) with a high work hardening rate response. This is the first computational plasticity calculation that accounts for grain size effects in a physically-based manner.

1. Introduction

The grain-size dependence of yield stress in metals has been represented as a $D^{-1/2}$ relationship since the pioneering work of Hall [1] and Petch [2]. The term Hall–Petch was introduced by Conrad [3] as a tribute to these researchers. The original explanation for this effect, envisaged by Hall and Petch, was that pile-ups formed at grain boundaries, and required a critical stress to break through them. The important contributions by Ashby [4], Hirth [5], and Thompson [6] strengthened the argument that causes other than pile-ups were responsible for the grain size effects. Clear evidence for the formation of a layer of high dislocation density in the direct vicinity of the grain boundaries, starting at an applied stress below the global yield stress, is the transmission electron microscopy by Murr and Hecker [7] (especially, Fig. 2). Meyers and Ashworth [8] proposed a mechanism based on elastic anisotropy of the grains. Nevertheless, pile-ups are still widely recognized as the dominating effect.

The Hall–Petch relationship has recently come under close scrutiny in the context of nanocrystalline materials, pioneered by Gleiter and co-workers [9,10]. Weertman and co-workers [11–14] have investigated the effect of grain size, in the nanocrystalline domain, on yield stress, in a systematic manner. Sample imperfections (voids, microcracks incomplete boundary of particles) masked many of the mechanical characteristics of nanocrystalline materials in early work, and careful processing and characterization has been needed to eliminate (or, at least, mitigate) these effects. A recent overview [14] presents the current thinking on this. Koch and co-workers [15–19] studied nanocrystalline iron; a focused effect was also undertaken to remove flaws (voids, microcracks, incomplete boundaries of particles, etc.) in order to obtain more reliable mechanical strength under both compression and tension. In summary, the experimental results indicate that the Hall–Petch slope in the nanocrystalline domain is lower than in the microcrystalline (conventional) range

* Corresponding author. Tel.: +1-858-5344719; fax: +1-858-5345698.

E-mail address: mameyers@mae.ucsd.edu (M.A. Meyers).

0921-5093/01/$ - see front matter
PII: S0921-5093(00)02029-3

of grain sizes. In some cases, a zero or even negative Hall–Petch slope has been reported [20]; however, this may well be an artifact of sample preparation.

2. Elastic anisotropy

A polycrystalline aggregate, upon being subjected to external tractions, develops a highly inhomogeneous state of internal stresses, due to the elastic anisotropy of the individual grains. Such inhomogeneous state of stress can only be avoided if the anisotropy ratio is one. For instance, for iron and copper, one has:

Fe	Cu
$E_{100} = 125$ GPa	$E_{100} = 67$ GPa
$E_{110} = 200$ GPa	$E_{110} = 130$ GPa
$E_{111} = 272$ GPa	$E_{111} = 190$ GPa

Fig. 1 shows a polycrystalline aggregate (Cu) subjected to compressive tractions through the uniform displacement of the end platens. The computational approach is described in Section 5.1. The average imposed stress, obtained by dividing the strain (set equal to 0.000225) by the polycrystalline Young's modulus (120 GPa), is equal to 27.9 MPa. The arrangement of grains is shown in Fig. 1(a). Three types of grains, with orientations [100], [110], and [111], are considered. They are white, gray, and black, respectively, in Fig. 1(a). The material is not truly anisotropic, because the individual grains are taken to be isotropic (but with different Young moduli). Figs. 1(b) and (c) show the principal stresses σ_1 and σ_2, and their variation through the section marked A–A. As expected, σ_1 fluctuates around zero, while σ_2 varies between -20 and -55 MPa. The maximum shear stress is shown in Fig. 1(d). It varies between 13 and 30 MPa. The shear stresses vary significantly throughout the grains.

3. Phenomenological model

A mechanism for the effect of grain size on the yield stress is presented here. It is essentially an extension of the model proposed by Meyers and Ashworth (MA) [8] to the nanocrystalline regime. This model does not

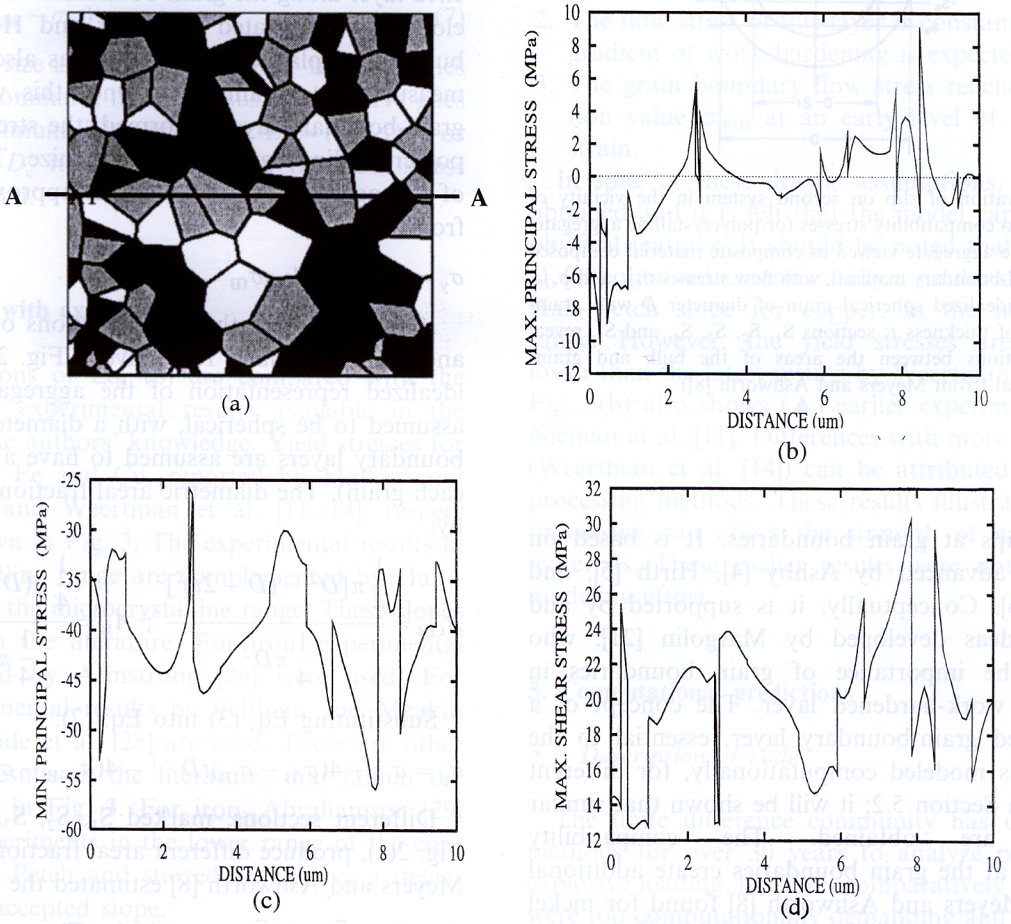

Fig. 1. Elastic stresses in polycrystalline copper loaded elastically; (a) grain configuration; three grain orientations: white [100], gray [110], and black [111]; (b) maximum principal stress (σ_1); (c) minimum principal stress (σ_2); (d) maximum shear stress.

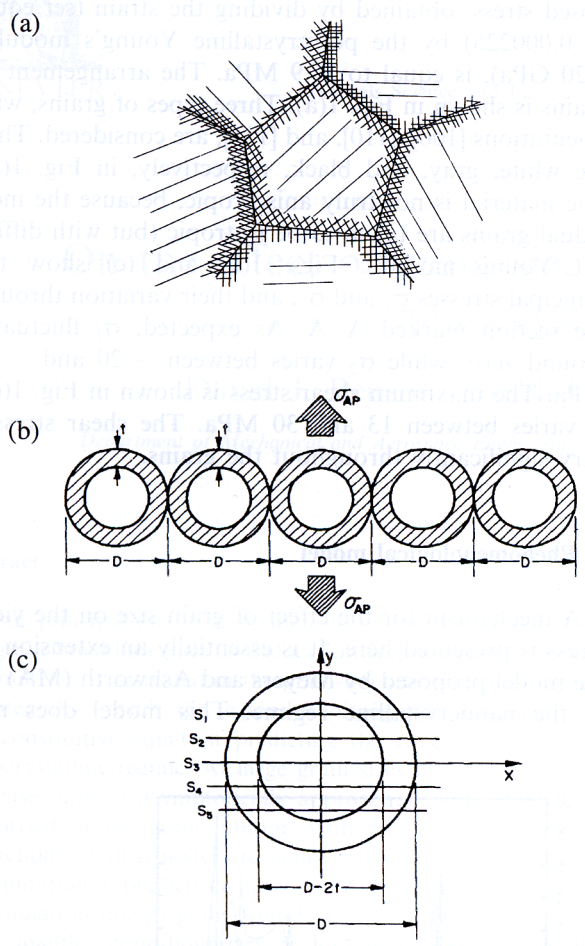

Fig. 2. (a) Activation of slip on second system in the vicinity of boundaries due to compatibility stresses for polycrystalline aggregate; (b) polycrystalline aggregate viewed as composite material composed of bulk and grain-boundary material, with flow stresses σ_{GB} and σ_{GB}, respectively; (c) idealized spherical grain of diameter D with grain-boundary layer of thickness t; sections S_1, S_2, S_3, S_4, and S_5, reveal different proportions between the areas of the bulk and grain-boundary material (from Meyers and Ashworth [8]).

require pile-ups at grain boundaries. It is based on earlier ideas advanced by Ashby [4], Hirth [5], and Thompson [6]. Conceptually, it is supported by and parallel to ideas developed by Margolin [21], who emphasizes the importance of grain boundaries in generating a work-hardened layer. The concept of a work-hardened grain-boundary layer, essential to the MA model, is modeled computationally, for different grain sizes, in Section 5.2; it will be shown that similar predictions are obtained. The compatibility requirements at the grain boundaries create additional stresses, τ_I. Meyers and Ashworth [8] found for nickel (by FEM calculations on a bicrystal) that

$$\tau_I = 1.37\sigma_{AP} \tag{1}$$

where σ_{AP} is the applied normal stress. In a uniform, homogeneous natural, $\tau = \sigma/2$. Thus, the shear stress at the interface is between two and three times the maximum shear stress in a homogeneous/uniform material. This is consistent with the result given in Section 2 for copper. It is therefore logical to expect the initiation of plastic flow to take place in the grain boundary regions. Other factors that contribute to this:

1. Grain boundaries are sources of dislocations. This is a well-known phenomenon; grain-boundary ledges and grain-boundary dislocations can initiate plastic deformation (e.g., Li and Chou [22], Murr [23], Sutton and Balluffi [24]).
2. Grain boundaries segregate impurities and foreign atoms and their mechanical properties differ from the grain interiors.
3. Dislocations pile up at grain boundaries.

As a result, while the grain interiors can be considered to harden by the classic easy glide/linear hardening/parabolic hardening sequence, the grain boundaries show a much faster rise in dislocation density.

The MA model is presented here in a shortened manner. As the applied stress increases, a work hardened layer along the grain boundaries is formed. This is eloquently illustrated by Murr and Hecker [7]. This build-up of plastic deformation has also been recently measured by Adams [25]. Once this work hardened grain-boundary layer is formed, the stresses within the polycrystalline aggregate homogenize. The flow stress of the aggregate is obtained, in approximate fashion, from:

$$\sigma_y = A_B\sigma_{fB} + A_{GB}\sigma_{fB} \tag{2}$$

A_B and A_{GB} are the areal fractions of grain interior and grain boundary, respectively. Fig. 2(b,c) shows an idealized representation of the aggregate. Grains are assumed to be spherical, with a diameter D; the grain boundary layers are assumed to have a thickness t (in each grain). The diametric areal fractions are expressed by:

$$A_{GB} = \frac{\frac{1}{4}\pi[D^2 - (D-2t)^2]}{\frac{1}{4}\pi D^2}\ ;\ A_B = \frac{\frac{1}{4}\pi(D-2t)^2}{\frac{1}{4}\pi D^2} \tag{3}$$

Substituting Eq. (3) into Eq. (2):

$$\sigma_y = \sigma_{fB} + 4(\sigma_{fB} - \sigma_{fB})tD^{-1} - 4(\sigma_{fGB} - \sigma_{fB})t^2D^{-2} \tag{4}$$

Different sections, marked S_1, S_2, S_3, S_4, and S_5 in Fig. 2(c), produce different areal fractions A_B and A_{GB}. Meyers and Ashworth [8] estimated the mean values of t and D, $\bar{t}$ and $\bar{D}$, respectively. They are $\bar{D} = \frac{\pi}{4}D$ and $\bar{t} = 1.57t$.

Hence, it is more correct to use these values. The ratio tD^{-1} is approximately equal to $2\bar{t}\bar{D}^{-1}$. Eq. (4) breaks down when $D \leq 2t$. The Hall–Petch dependency, universally obtained for large grain sizes, can be inserted into Eq. (4) by establishing a functional dependence of t of the form:

$$t = k_{MA} D^{1/2} \tag{5}$$

The rationale for this relationship is the following. There are two effects: (a) as the grain size is decreased, the stress field fluctuations vary with D. This would lead to a dependency $t = k_1 D$; (b) the dislocation spacing is unchanged and the dislocation interactions will dictate a constancy in t; thus, a relationship $t = k_2 D^0$. The geometric mean would be: $(k_1 k_2 D)^{1/2}$, or $k_{MA} D^{1/2}$.

Substituting Eq. (5) into a modified form of Eq. (4) and taking the terms $\bar{D}$ and $\bar{t}$ into account:

$$\sigma_y = \sigma_{fB} + 8k_{MA}(\sigma_{fGB} - \sigma_{fB})\bar{D}^{-1/2} - 16k_{MA}^2(\sigma_{fGB} - \sigma_{fB})\bar{D}^{-1} \tag{6}$$

For large grain sizes (in the micrometer range) the $D^{-1/2}$ term dominates and a Hall–Petch relationship is obtained. The Hall–Petch slope, k_{HP}, is equal to:

$$k_{HP} = 8k_{MA}(\sigma_{fGB} - \sigma_{fB}) \tag{7}$$

As the grain size is decreased, the D^{-1} term becomes progressively dominant; the σ_y versus $D^{-1/2}$ curve goes through a maximum. This occurs at $D_c = (4k_{MA})^2$ For values of $D < D_c$ it is assumed that the flow stress reaches a plateau.

4. Comparison with experiments

The predictions of Eq. (6) are compared with the most extensive experimental results available in the literature, to the authors' knowledge. Yield stresses for nanocrystalline Fe and Cu, reported by Mallow and Koch [17,18], and Weertman et al. [11–14], respectively, are shown in Fig. 3. The experimental results in the nanocrystalline range are complemented by Hall–Petch slopes in the microcrystalline range. These slopes are reported in the literature. For iron, experimental results reported by Armstrong [26] were used. For copper, experimental results by Feltham and Meakin [27] and Andrade et al. [28] are used. There are other experimental results in the literature, that fall in the range reported in Fig. 3. For iron, Abrahamson [29] carried out experiments in the lower range of the conventional Hall–Petch and started to observe a deviation from the accepted slope.

It is clear, for both Fe and Cu, that the σ_y versus $D^{-1/2}$ relationship is not linear over the range millimeter–nanometer. The Hall–Petch line is an approximation that is effective in the mm–μm range. There is strong evidence that the slope decreases and that the curve asymptotically approaches a plateau when the grain size is progressively reduced. Eq. (6) is successful in representing the principal features experimentally observed. Three parameters have to be established: σ_{fB}, σ_{fGB}, and k_{MA}. σ_{fB} is the saturation stress and represents the flow stress of the work hardened grain-boundary layer. It is taken as the maximum of the yield stress. k_{MA} is obtained by conversion of k_{HP} according to Eq. (7). This ensures a good match between HP and MA for large grain sizes. Table 1 shows the parameters used in the calculation. The continuous curves in Fig. 3 represent the application of Eq. (6); a reasonable fit is obtained and the principal features are captured. For grain sizes below the maximum of the flow stress in the MA equation, a straight horizontal line is taken; in this regime, the grain boundaries (σ_{fGB}) dominate the process.

There are many simplifications and assumptions in this model. The most prominent are:

1. The work hardened layer t is assumed to have a grain size dependence of $D^{-1/2}$ This assumption is based on the σ_y versus $D^{-1/2}$ dependence.
2. The flow stress of this layer is constant. In reality, a gradient of work hardening is expected.
3. The grain boundary flow stress reaches the saturation value σ_{fGB} at an early level of global plastic strain.

In spite of these drastic assumptions, a good fit is obtained and it is felt that the model captures the key physical features. It should be noted that Gertsman et al. [30] obtained experimentally a similar decrease in the Hall–Petch slope for copper, in the nanocrystalline range. However, the yield stresses are significantly lower than the latest results by Weertman et al. [13,14]. Fig. 3(b) also shows (▲) earlier experimental data by Nieman et al. [11]. Differences with more recent results (Weertman et al. [14]) can be attributed to improved processing methods. These results illustrate how much processing can affect the strength of nanocrystalline materials. These earlier results were not used in the modeling effort.

5. Computational predictions

5.1. Description of code

The finite difference community has used Eulerian methods for over 30 years to analyze problems with explosive loading, but until comparatively recently, they were too computationally demanding and inaccurate to be attractive for solving problems in solid mechanics. The calculations in this research were performed with

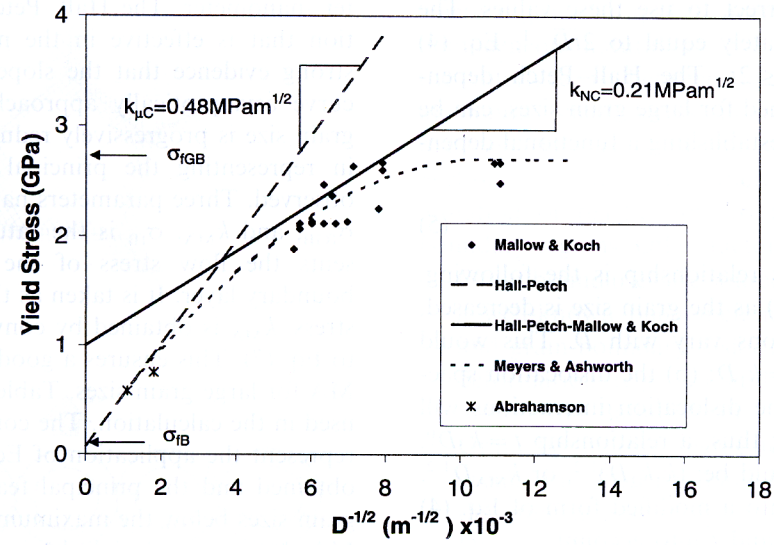

(a)

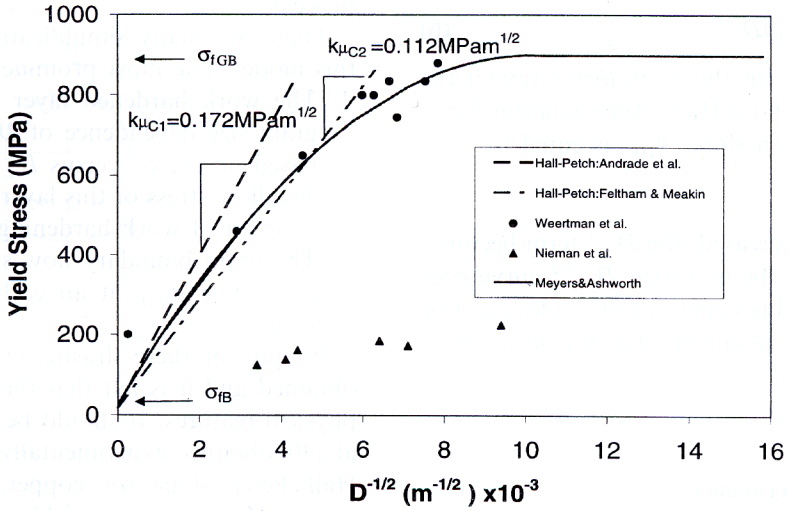

(b)

Fig. 3. σ_y versus $D^{-1/2}$ relationship for (a) iron and (b) copper; comparison of experimental results and predictions of Eq. (7).

Raven, an explicit, multi-material Eulerian program developed by Benson for research in materials science and manufacturing. It uses the van Leer MUSCL algorithm [31] for the material transport while the Lagrangian part of the code follows the standard formulation used in most explicit finite element codes. A comprehensive review paper by Benson [32] discusses the algorithms in greater detail.

5.2. Results of computations

For computational calculations, realistic polycrystals were used. Four grain sizes were modeled: 100, 10, 1, and 0.1 μm. The thickness of the grain-boundary layer, t, was varied and the respective values used are: 3.75, 0.75, 0.15, and 0.03 μm. The material chosen for the modeling effort is copper, because of the significant amount of information on grain-size effects available (see Fig. 3(b)). The microstructures, already divided into grain interiors and grain-boundary layers, are shown in Fig. 4. For the largest grain size modeled (100 μm), the grain-boundary region is barely distinguishable, whereas for the smallest grain size (0.1 μm), the grain-boundary region occupies a significant portion.

Table 1
Parameters used for MA model

	σ_{fB} (MPa)	σ_{fGB} (MPa)	k_{Hp} (MPa m$^{1/2}$)	k_{MA} (m$^{1/2}$)
Fe	100	2800	0.48	2.2×10^{-5}
Cu	25	900	0.112–0.172	$(1.6–2.4)\times10^{-5}$

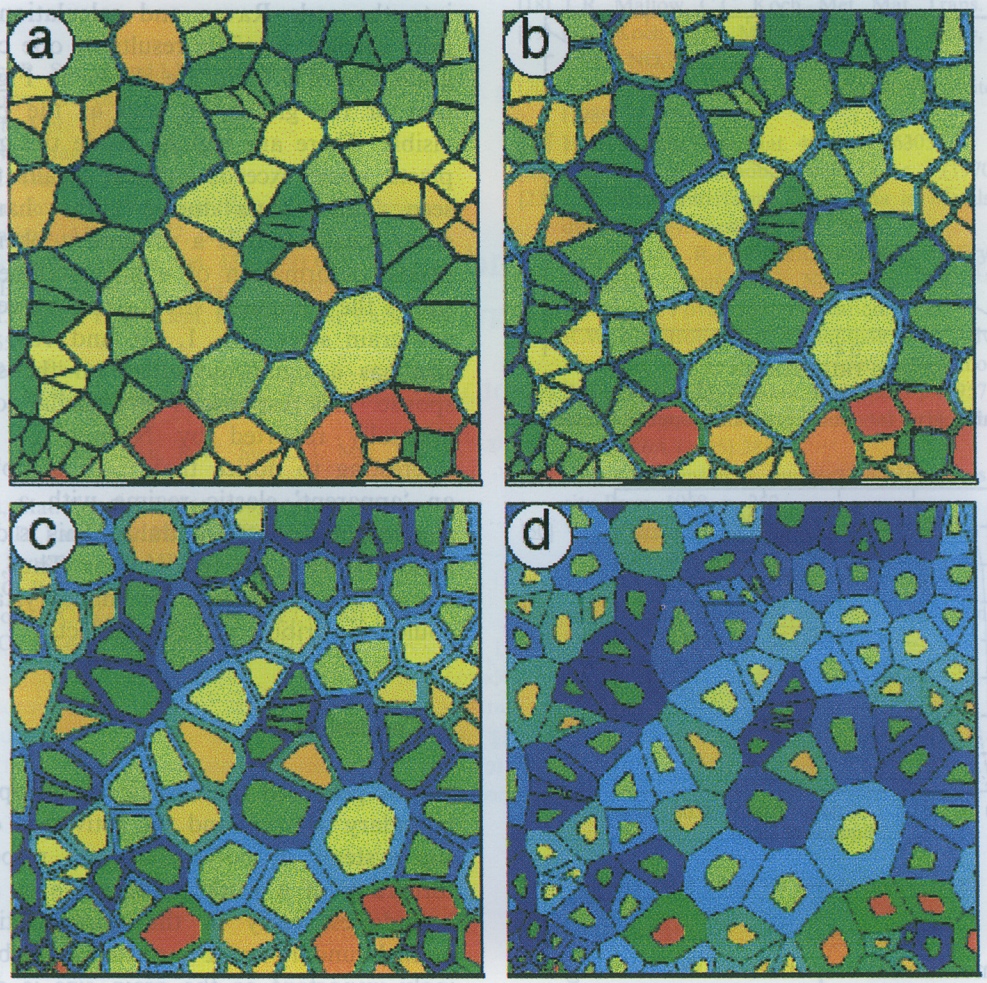

Fig. 4

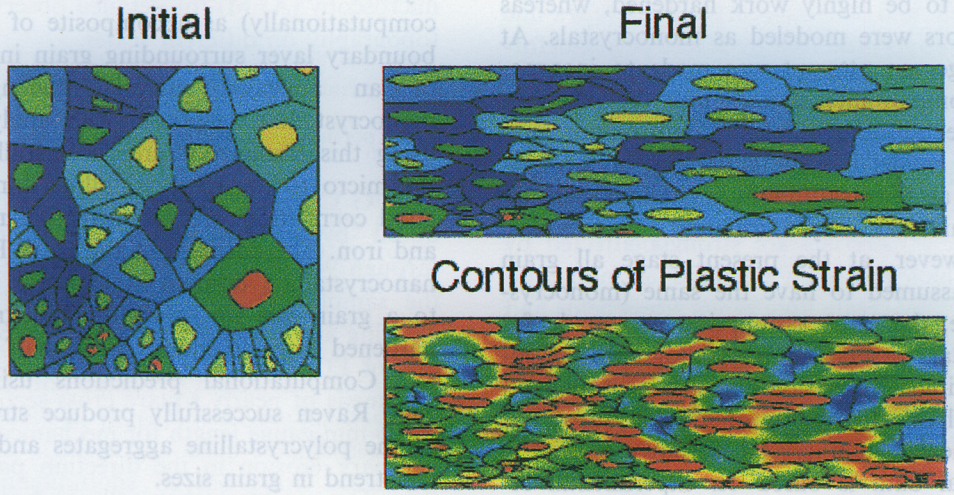

Fig. 6

Fig. 4. Simulated polycrystalline aggregate used in computations; (a) $D = 100$ μm, $t = 3.75$ μm; (b) $D = 10$ μm, $t = 0.75$ μm; (c) $D = 1$ μm, $t = 0.15$ μm; (d) $D = 0.1$ μm, $t = 0.03$ μm.

Fig. 6. The initial and final state with contours of the equivalent plastic strain for the microstructure with the 0.1 μm grain size. The contours range from blue for no plastic strain to red for plastic strain levels greater than 1.0.

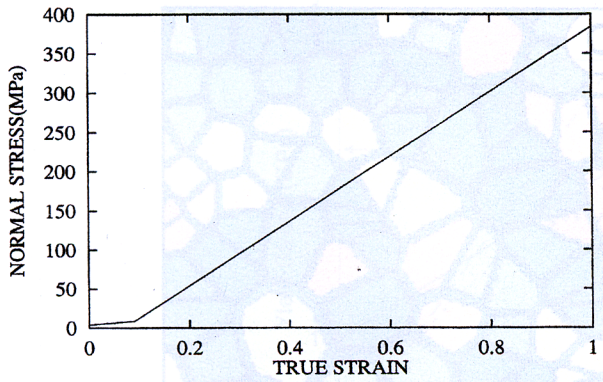

Fig. 5. Stress–strain curve for monocrystalline copper representing grain interior.

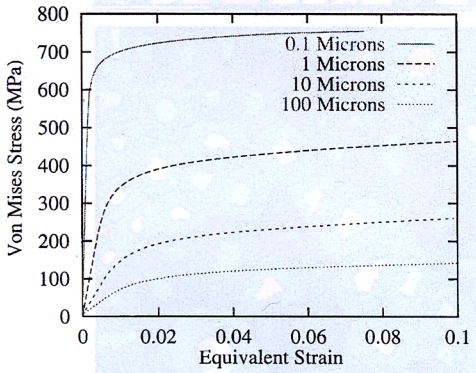

Fig. 7. Calculated stress–strain curves for grain sizes ranging from 0.1 to 100 μm.

The different mechanical responses of the two regions were also incorporated. The grain-boundary region was considered to be highly work hardened, whereas the grain interiors were modeled as monocrystals. At the present stage, no attempt was made to incorporate elastic incompatibility stresses into the plasticity analysis and the build-up of plastic deformation into the model. The model has the capability of incorporating as many as fifteen different crystallographic directions (manifested by different mechanical responses). However, at the present stage all grain interiors were assumed to have the same (monocrystalline) response; the same assumption was made for the grain-boundary layers. The crystallographic orientation and specimen dimensions have a profound effect on the mechanical response of monocrystals. The response of annealed monocrystal is shown in Fig. 5. The monocrystal data is based on experimental results reported by Diehl [33] and represents an average; a bilinear stress–strain response is assumed (Fig. 5) that captures both the easy glide and linear hardening stages of work hardening. The work-hardened grain-boundary region was assumed to respond as a perfectly plastic material with a flow stress of 900 MPa (this value is identical to the one from Table 1). These two stress–strain responses were incorporated into the code Raven and calculations were successfully carried out. The results of one calculation for a grain size of 0.1 μm are shown in Fig. 6. The distortion of the grains, as well as the plastic strain, is visible. There are regions inside the grains where the plastic strain exceeds 1. Shear localization can also be seen. This occurs during global hardening. Indeed shear localization is a prominent phenomenon in the plastic deformation of nanocrystalline metals. Fig. 7 shows the computed stress-strain curves for the different grain sizes (0.1, 1, 10, and 100 μm). The grain size has a significant effect on the stress–strain response. This response is very similar to the one experimentally reported by Nieman et al. [11]. It is interesting to notice that these computations predict an 'apparent' elastic regime with a slope that is a fraction of Young's modulus. This is due to the interaction between the two regions. Thus, the lower elastic moduli observed for nanocrystalline materials could be attributed to these effects.

6. Conclusions

It is proposed that elastic anisotropic effects, grain boundary sources, and the activation of two or more slip systems in polycrystals are responsible for the formation of a work hardened layer along the grain boundaries, early in the microplastic region. This grain boundary work-hardened layer becomes increasingly important as the grain size is decreased. Polycrystals are modeled (both analytically and computationally) as a composite of a work-hardened boundary layer surrounding grain interiors comprised of an annealed material having a essentially monocrystalline response. The analytical predictions using this framework are successfully extended from the micro to the nanocrystalline domain and show a good correlation with experimental results for copper and iron. The decrease of the Hall–Petch slope in the nanocrystalline domain is captured and corresponds to a grain size for which the thickness of the work hardened layer is equal to one half the grain diameter. Computational predictions using the Eulerian code Raven successfully produce stress–strain curves of the polycrystalline aggregates and predict the correct trend in grain sizes.

Acknowledgements

This research was supported by the US Army Research Office Multidisciplinary University Research Initiative (Contract No. DAAH 04-96-1-0376) and NSF grant (DMI-9612017).

References

[1] E.O. Hall, Proc. R. Soc. (Lond.) B64 (1951) 9474.
[2] N.J. Petch, J. Iron Steel Inst. 174 (1953) 25.
[3] H. Conrad, Acta Met. 11 (1963) 75.
[4] M.F. Ashby, Phil. Mag. 21 (1970) 399.
[5] J.P. Hirth, Met. Trans. 3 (1972) 61.
[6] A.W. Thompson, in: A.W. Thompson (Ed.), Work Hardening in Tension and Fatigue, AIME, 1977, p. 399.
[7] L.E. Murr, S.S. Hecker, Scripta Met. 13 (1979) 667.
[8] M.A. Meyers, E. Ashworth, Phil. Mag. A46 (1982) 737.
[9] R. Birringer, H. Gleiter, H.-P. Klein, P. Marquardt, Phys. Lett. 102A (1984) 365.
[10] H. Gleiter, Z. Metallk. 86 (1995) 78.
[11] G.W. Nieman, J.R. Weertman, R.W. Siegel, Scripta Met. Mat. 24 (1990) 145.
[12] G.W. Nieman, J.R. Weertman, R.W. Siegel, J. Mat. Res. 6 (1991) 1012.
[13] J.R. Weertman, Mat. Sci. Eng. A166 (1993) 161.
[14] J.R. Weertman, D. Farkas, K. Hemker, H. Kung, M. Mayo, R. Mitra, H. Van Swygenhoven, MRS Bulletin 24 (1999) 44.
[15] J.S.C. Jang, C.C. Koch, Scripta Mat. 24 (1990) 1599.
[16] R.O. Scattergood, C.C. Koch, Scripta Met. 27 (1992) 1195.
[17] T.R. Mallow, C.C. Koch, Acta Mat. 45 (1997) 2177.
[18] T.R. Mallow, C.C. Koch, Met. Mat. Trans. 29A (1998) 2285.
[19] C.C. Koch, D.G. Morris, K. Lu, A. Inoue, MRS Bulletin 24 (1999) NO.255.
[20] A.H. Chokshi, A.S. Rosen, J. Karch, H. Gleiter, Scripta Met. 23 (1989) 1679.
[21] H. Margolin, Acta Mat. 46 (1998) 6305.
[22] J.C.M. Li, Y.T. Chou, Metall. Trans. 1 (1970) 1145.
[23] L.E. Murr, Interfacial Phenomena in Metals and Alloys, Addison Wesley, Reading, MA, 1975.
[24] A.P. Sutton, R.F. Baluffi, Interfaces in Crystalline Materials, Oxford University Press, New York, 1994.
[25] B. Adams, Private communication, 1999.
[26] R.W. Armstrong, in: R.F. Bunshah (Ed.), Advances in Materials Research, vol. 5, Wiley-Interscience, New York, 1971, p. 101.
[27] P. Feltham, J.D. Meakin, Phil. Mag. 2 (1957) 105.
[28] M.A. Meyers, U.R. de Andrade, A.H. Chokshi, Met. Mat. Trans. 26A (1995) 2881.
[29] E.P. Abrahamson II, Surfaces and Interfaces, Syracuse University Press, 1968, p. 262.
[30] V.Y. Gertsman, M. Hoffmann, H. Gleiter, R. Birringer, Acta Mat. 42 (1994) 3539.
[31] B. van Leer, J. Comp. Phys. 23 (1977) 276.
[32] D.J. Benson, Comp. Meth. Appl. Mech. Eng. 999 (1992) 235.
[33] J. Diehl, Z. Metallk. 47 (1956) 331.